Spring 4-15-2011

Electrowetting Induced Cassie-Wenzel Transition on Textured Surfaces

Kenza Mouttaki
University of South Florida

Electrowetting Induced Cassie-Wenzel Transition on Textured Surfaces

by

Kenza Mouttaki

A thesis submitted in partial fulfillment
of the requirements for the degree
of Bachelors in Mechanical Engineering
College of Engineering
Honors College
University of South Florida

Professor: Nathan Crane

Date of Approval:
April 15th , 2011

Acknowledgement

This thesis would not have been possible without the support, help and guidance of several individuals who have contributed and extended their valuable assistance in the research fabrication steps and the thesis preparation.

First and foremost, my mentor Dr. Nathan Crane, Assistant Professor in Mechanical Engineering at the University of South Florida who has provided the research environment and helped me through every step of the process. Dr. Crane has been a great advisor and supported me through the ups and downs, the moments of excitement and the stressful times. Without him this research would not have taken place and this thesis would not have lieu.

Dr. Kleine and Dr. Silverman without whom the Honors College will not be what it is today, a college that empowers students of different backgrounds in achieving their goals and dreams, a college that provides the moral support needed, the accommodation and space needed by the students. My utmost gratitude to the entire staff of the Honors College whose help I will never forget.

Jose Carballo Boschetti whose help with the fabrication of the substrates has been key to this research.

Hasnaa Mouttaki for her patience and reliable explanation of chemical properties and chemical reactions between compounds of interest.

Last but not least, I would like to thank my family for the continuous support, love and care, without them I would not be where I am today. They have each given me the strength to plod on despite my desire to give up and throw in the towel, thank you so much my beloveds.

Table of Content

ABSTRACT i

ABBREVIATION ii

LIST OF TABLES iii

LIST OF FIGURES iv

CHAPTER 1 INTRODUCTION 1

1.1 Motivation for Research.....1

1.2 Electrowetting 2

1.3 Hysteresis and Contact Angle.....4

1.4 Cassie-Baxter and Wenzel Law.....5

CHAPTER 2 FABRICATION.....9

2.1 Photolithography.....9

2.2 Deep Reactive Ion Etch – DRIE.....11

2.3 Cleaning.....12

2.4 Fluoropolymer Deposition.....15

CHAPTER 3 PROCEDURE & RESULTS.....17

3.1 Procedure.....17

3.2 Results and Discussion.....18

CHAPTER 4 CONCLUSION.....23

REFERENCES 25

APPENDICES.....28

Abstract

The electrowetting field expanded drastically during the last decade. It combines several laws and theories out of which Young's equation, Cassie law and Wenzel law. The main focus of electrowetting is the transition between a superhydrophobic state -Cassie- and a hydrophilic state -Wenzel-. This transition allows a wide range of applications such as microfluidics, lab-on-a-chip devices, chemical microreactors and management of microelectronics.

The purpose of this research is to provide a standard operational procedure for the fabrication of substrates that allow the Cassie to Wenzel transition. Theoretical equations are compared to experimental results. These substrates will be implemented in future research projects. The substrates consist of micro-size posts etched at two different depths, with a semi-conducting silicon oxide surface layer and coated with a commercial fluoropolymer. They are tested using water droplets. After series of tests, we concluded that experimental results match the expected results and that the wafers can be implemented in different applications.

Abbreviation

HMDS	Hexamethyldisilazane
DRIE	Deep Reactive Ion Etch
RIE	Reactive Ion Etch
RCA	Radio Corporation of America
BOE	Buffered Oxide Etch
SEM	Scanning Electron Microscope

List of Tables

Table 1. Voltage versus angle response on 100 µm deep posts.....20

Table 2. Angle measurements on both 10 µm and 100 µm deep posts.....21

Table A.1. Roughness and Cassie Coefficient for 10 µm deep posts.....28

Table A.2. Roughness and Cassie Coefficient for 100 µm deep posts.....28

Table A.3. Ratios of diameter to pitch.....28

Table B.1. Expected Cassie and Wenzel angles versus Voltage on 10 µm.....29

Table B.2. Expected Cassie and Wenzel angles versus Voltage on 100 µm.....29

List of Figures

Figure 1. Illustration of interfacial tensions.....6

Figure 2. Top plane view (on left) and side view of a square lattice (on right).....6

Figure 3. Photolithography mask.....9

Figure 4. Photolithography setup.....10

Figure 5. Isotropic wet etch (left), anisotropic wet etch (middle) and DRIE straight wall etch (right).....11

Figure 6. SEM pictures.....15

Figure 7. Goniometer.....17

Figure 8. Graph showing roughness versus Cassie coefficient.....18

Figure 9. Pictures of Cassie-Wenzel transition on 10µm deep posts. Contact angle measurement: a) 138 degrees, b) 112 degrees, c)95 degrees, d) 63 degrees.....19

Figure 10. Pictures of Cassie-Wenzel transition on 100µm deep posts. Contact angle measurement: a) 148 degrees, b) 122 degrees, c)64 degrees, d) 33 degrees.....19

Figure 11. Expected Cassie, expected Wenzel and experimental results of voltage versus contact angle on 10 µm deep posts.....21

Figure 12. Expected Cassie, expected Wenzel and experimental results of voltage versus contact angle on 100 µm deep posts.....22

1. Introduction

1.1 Motivation for Research

The electrowetting field expanded drastically during the last decade because of its ability to revive older theories pertinent to challenge future applications. This research field has seen 70% annual growth in patents and publications since 2001[1]. Electrowetting combines several laws and theories out of which Young's equation, Cassie law and Wenzel law. The main focus of electrowetting is the transition between Cassie and Wenzel states which is also referred to as the transition between the superhydrophobic and hydrophilic states.

Superhydrophobic surfaces have extremely high contact angle and remarkable interfacial properties and very low flow resistance as well as the ability to self-clean. They are the subject of interest of both the academic and industrial research worlds. These properties allow a wide range of applications such as microfluidics, lab-on-a-chip devices, chemical microreactors and thermal management of microelectronics[5].

Wenzel law describes the linear relation between surface roughness and contact angle. The Wenzel state refers to the homogeneous wetting regime. Cassie law is a more complex relation that describes the relation between the contact angle and a heterogeneous substrate; the higher the former is, the higher the latter will be. The Cassie state refers to the superhydrophobic state where the liquid forms an ideal straight angle with the substrate.

Young's equation on surface energy is considered the substratum of all wetting theory; it is the interaction between the forces of cohesion and those of adhesion which determines the

occurrence of the wetting phenomena[3]. This equation assumes an ideal perfectly flat surface to describe the contact angle as a function of the surface free energy.

It has been shown very significant to dynamically control the interaction of liquids with the superhydrophobic surfaces; modifying the contact angle as well as tuning the degree of penetration in the surface. Effective dynamic tuning has been reported a few years ago, yet the transition from superhydrophobic to hydrophilic behavior was considered irreversible at the time[5]. It was later shown that the application of a difference in potential between the liquid and the substrate, induced pulse or oil allows the reversibility[1].

For the purpose of this thesis, the contact angle of the electrically-controlled reversible wetting-dewetting transition on superhydrophobic microstructures will be inspected. Theoretical results show a decrease from the hydrophobic (>150˚) contact angle to the hydrophilic (<100˚) contact angle[1]. This research will compare theoretical results which can be predicted using energy minimization, interfacial thermodynamics or electromechanics, to experimental results of the contact angle on silicon oxide microposts topped with a fluoropolymer to provide the hydrophobicity for the Cassie state.

1.2 Electrowetting

Electrowetting involves application of electrical potential across a liquid/dielectric/electrode capacitor, a charge-induced imbalance of forces near the liquid/dielectric contact line and a resulting decrease in the observed liquid contact angle[1].

The basic electrowetting structure consists of a liquid droplet sitting on a fluoropolymer dielectric coated substrate charged by a Direct Current (DC) voltage source[1]. Energy minimization, interfacial thermodynamics or electromechanics can be used to predict theoretical results. The

difference in potential applied to the system allows the droplet/dielectric capacitor to recharge. These charges can consist of ionized water or an ionic surfactant (Sodium Dodecyl sulfate or ionized salt.) The electrical field is the result of the charge density close to the contact line.

In the context of this research, the substrate consists of micro-sized posts also referred to as micro-grass. The substrate is an electrical semi-conductor with a high-performance dielectric thin oxide surface layer dip-coated with a commercial hydrophobic fluoropolymer. The droplet consists of de-ionized water. In this case, the water droplet sits on top of the hydrophobic posts as well as the air that fills the space between the posts; this is referred to as the Cassie state where the meniscus is convex between the posts. "This convex meniscus has a corresponding Young-Laplace ($\Delta p \propto 2\gamma SA/r$) pressure that prevents liquid from wetting into the space between the posts;" [1] where γ is the interfacial tension, S is the three phase saline and A is ambient. On one hand, to counteract the gravitational forces and pressures that might cause the droplet to wet the space between the posts, the spacing between the posts has to be small; this spacing is also referred to as the pitch is ideally measured in micrometers. On the other hand, to achieve the Cassie state the surface fraction of the droplet in contact with the low surface energy posts should be less than the fractional area in contact with air.

The transition between the superhydrophobic Cassie state and the hydrophilic Wenzel state happens when the difference in potential is applied; the more the voltage is the increased, the more the electromechanical force will promote capillary wetting between the posts which will decrease the contact angle even more[5].

In theory, "if the advancement of the saline meniscus between the posts does not reach the bottom surface, and if the contact angle hysteresis is small, removing the voltage could lead to reversibility of wetting as the Young–Laplace pressure drives the liquid from between the posts.

For substrates with very small structures (≈µm) this situation is most often hypothetical since the electrowetting occurs in milliseconds or less and the saline quickly reaches the lower substrate surface." [1] Therefore, in practice the application of sufficient voltage leads the droplet to quickly reach the bottom surface of the substrate and wet the surface between the posts.

1.3 Hysteresis and Contact Angle

As previously presented, the wetting phenomena is governed by Young, Wenzel and Cassie-Baxter equations. The first equation –Young's- comes as a result of the equilibrium of forces acting on the triple line. The second and third equations provide the value of apparent contact angles inherent to rough surfaces[7].

There remains a factor involved in the wetting phenomena which makes it harder to understand; the effect of hysteresis of the contact angle. The contact angle is the angle at which the droplet meets the rough surface. On an ideal hydrophilic surface, a droplet wets the surface creating a 0˚ contact angle. On highly hydrophilic surfaces, the contact angle is measured between 0˚ and 30˚. On certain hydrophilic surfaces, the contact angle can be measured up to 90˚. On hydrophobic surfaces however, the contact angle is measured at 90˚ and higher. For the purpose of this research, superhydrophobic surfaces with contact angles of 150˚ and higher are implemented. These angles are measured using a contact angle goniometer.

Hysteresis however is not measurable yet quantifies as the difference between two types of angles: advancing and receding contact angle. The greater difference implies higher difference. While only one is favorable, there are two common methods for measuring the advancing and receding contact angles: the tilting base method and the add/remove method. The tilting method being the favorable one consists of dispensing a droplet on top of a leveled surface and tilting the

latter from 0˚ to 90˚. During the tilting, the downhill side will be in a wetting phase while the opposite side will be in a dewetting phase. The wetting angle will increase and represents the advancing angle. The dewetting angle is called the receding angle. The values of these angles are calculated right before the drop releases.

The Cassie state provides large contact angles and low hysteresis of drops on rough surfaces. Hysteresis is usually simplified in the ability of a drop to slide off an inclined surface[7]. High hysteresis means higher attraction of the drop to the rough surface. In the superhydrophobic Cassie state, the low hysteresis allows the drop to move around easily. In the hydrophilic Wenzel state however, "the fluid impales the grooves of the roughness features thus making the drop sticky" [7]. The Cassie and Wenzel formulas allow to identify the type of roughness geometries that lead to the Cassie State. The drop in the superhydrophobic state still exhibits hysteresis yet lower than that in the hydrophilic state.

1.4 Cassie-Baxter and Wenzel Law

As previously mentioned, Young's law defines the contact angle on a substrate material as[6]

$$\cos\theta = \frac{\gamma_{SG} - \gamma_{SL}}{\gamma_{LG}} \qquad \text{Eq.(1)}$$

where γ_{SL}, γ_{LV}, and γ_{SV} are the interfacial tensions between the solid and the liquid, the liquid and the vapor, and the solid and the vapor, respectively.

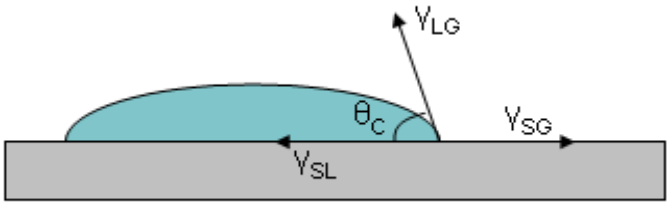

Fig. 1 Illustration of interfacial tensions

In the Wenzel state, the equation becomes

$$\cos\theta_W = r\cos\theta \qquad \text{Eq.(2)}$$

Where θ_w is the Wenzel contact angle and r is the roughness of the surface. In the Cassie state, the equation becomes

$$\cos\theta_C = f\cos\theta + (1-f)\cos\theta_0 \qquad \text{Eq.(3)}$$

where θ_0 is the contact angle with the layer of air and f is the ratio of contact surface to the total horizontal surface. An ideal Cassie state is $\theta_0 = \pi$; the equation can then be simplified to

$$\cos\theta_C = -1 + f(1+\cos\theta) \qquad \text{Eq.(4)}$$

For ease of calculation and modeling, we considered the square lattice shown in fig. 2 in order to calculate the Cassie and the Wenzel angle as well as the angle at which the transition occurs.

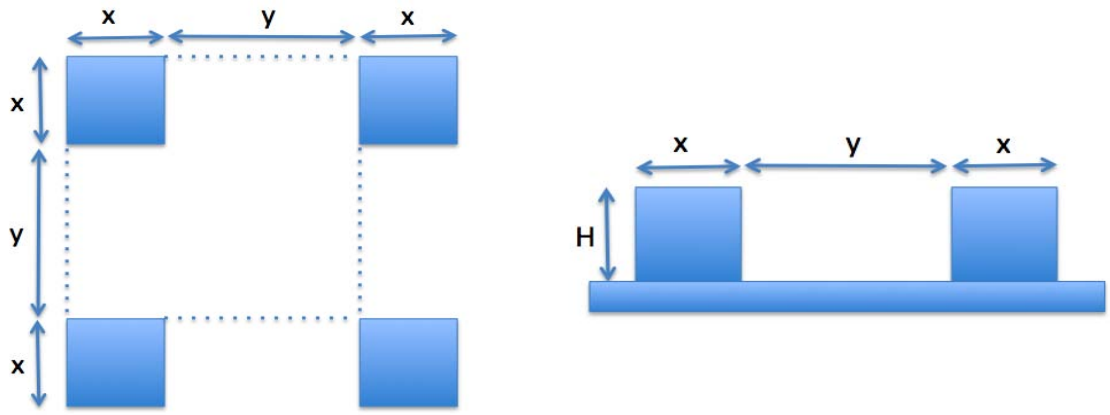

Fig. 2 Top plane view (on left) and side view of a square lattice (on right)

In the book “Micro-drops and Digital Microfluidics,” Jean Berthier gives an example of a sessile drop sitting on a square lattice. The surface roughness is considered as the ratio of the total surface to the horizontal surface, which leads to

$$r = \frac{(x+y)^2 + 4xH}{(x+y)^2} = 1 + \frac{4A}{(x/H)} \qquad \text{Eq.(5)}$$

where

$$A = \left(\frac{x}{x+y}\right)^2 \qquad \text{Eq.(6)}$$

The Cassie coefficient *f* is the ratio of surface of the top of the posts to the horizontal surface and is given by

$$f = \frac{x^2}{(x+y)^2} = A \qquad \text{Eq.(7)}$$

therefore the Wenzel angle is

$$\cos\theta_W = \cos\theta\left[1 + \frac{4A}{(x/H)}\right] \qquad \text{Eq.(8)}$$

the Cassie angle is

$$\cos\theta_C = -1 + A(1+\cos\theta) \qquad \text{Eq.(9)}$$

the angle at which the transition occurs is

$$\cos\theta_S = \frac{-1}{1 + 4\frac{xH}{y^2}} \qquad \text{Eq.(10)}$$

From these equations, we can conclude that the smaller the height of the pillars, the larger is the transition angle between the two states and therefore, the drop reaches the Wenzel state. Also,

when the pillars are thin (x goes to 0) the Area (A) goes to zero and so does the ratio of contact surface to the total surface (f); there the Wenzel state is attained. Finally, when the pillars are closer to one another (smaller pitch y), θ_i gets smaller and we observe the Cassie state[6].

Once the voltage is applied, the Cassie and Wenzel contact angles can be calculated using the following equations[40, 41]:

$$\cos\theta_C^E = -1 + f\left(1 + \cos\theta_0 + \eta\right) \qquad \text{Eq.(11)}$$

$$\cos\theta_W^E = \cos\theta_0 + \eta \qquad \text{Eq.(12)}$$

with

$$\eta = \frac{k\varepsilon_0 V^2}{2t\gamma_{LG}} \qquad \text{Eq.(13)}$$

where t is the dielectric layer thickness, $k\varepsilon_0$ is the dielectric capacitance and V is the applied voltage.

2. Fabrication

The fabrication of the posts consists of four major steps: photolithography consisting of transferring the pattern from a mask onto the wafer, etching the posts, growing an oxide layer and depositing a hydrophobic fluoropolymer layer.

2.1 Photolithography

"Photolithography is the process of transferring geometric shapes on a mask to the surface of a silicon wafer."[9] This process consists of six mandatory steps for the obtainment of a good resistive pattern.

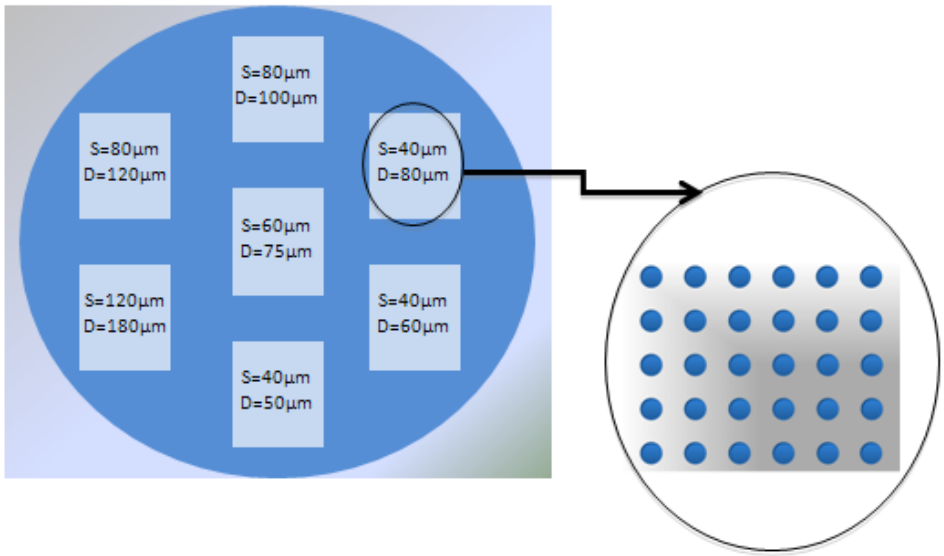

Fig. 3 Photolithography mask

The first step consists of cleaning the silicon wafer with Acetone, Methanol, Isopropanol and Water consequently, then drying it with Nitrogen. The second step is the application of a barrier layer; ideally, a thin layer of Hexamethyldisilazane HMDS of a few microns helps the photoresist adhere to the surface of the wafer. The wafer is softly baked at a temperature of

110°C for 85 seconds. A layer of AZ-4620 photoresist of 7.5 microns in thickness is deposited using the same techniques; spinning at 5 different ramping steps for a total of 95 seconds. It first ramps up to 1500rpm in 10 seconds, steps up to 2000 rpm and maintains for 60 seconds, it then steps down to 500 rpm and maintains for 10 seconds, it then steps up to 1000 rpm maintains for 10 seconds to finally ramp down to 0 rpm in 5 seconds. The next step consists of soft baking the wafer a second time which allows dehumidifying the thick and dense layer of AZ-4620 photoresist, and adhering more to the wafer. The wafer undergoes a moisture treatment for one hour before development; it is placed in boxed box with a damp towel. The wafer is then carefully placed under the optical lithography machine which emits an ultraviolet light through the mask onto the wafer; this makes specific areas of the photoresist insoluble to the developer. There are two types of photoresist: positive and negative. AZ-4620 is a positive photoresist and is most suited for the etching process. A common catch-phrase is used to remember the combination of mask and photoresist that should be used; for positive photoresist, *what shows goes,* and therefore for a negative photoresist, the opposite applies.

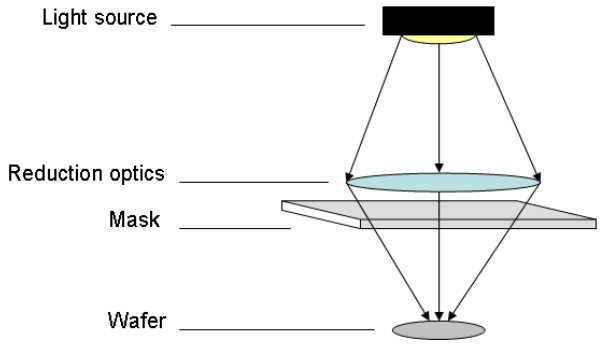

Fig. 4 Photolithography setup

The wafer is exposed for 63 seconds at 25 mW/cm^2. The next step consists of developing the wafer; a diluted solution of AZ-400 is used. The wafer is dipped in the developer and slowly

stirred for two minutes. The rotational motion helps the developer reach between the posts and remove the non-exposed/soluble photoresist. The developing reaction is ended by method of overflow where the wafer is dipped in a beaker filled with overflowing water. After the wafer is dried with nitrogen, it is inspected under the microscope. It is mandatory to keep the area clean from dust or other organic residue that could interfere with the desired pattern that is why this procedure is done in a clean room with special lighting in order to keep the photoresist from unwanted UV-light exposure.

2.2 Deep Reactive Ion Etch - DRIE

The patterned wafer is then etched in order to obtain the desired depth of posts. These posts require a high aspect ratio, a steep side with a perfect 90˚ angle because of this we use Deep Reactive Ion Etch (DRIE) method. Unlike the traditional Reactive Ion Etch (RIE), DRIE allows to create deep, steep-sided trenches of high-aspect ratio in a silicon wafer. Indeed, as shown in fig.6, RIE etches in a curved shape as the wafer is submerged in a solution and the etching is not vertically controlled.

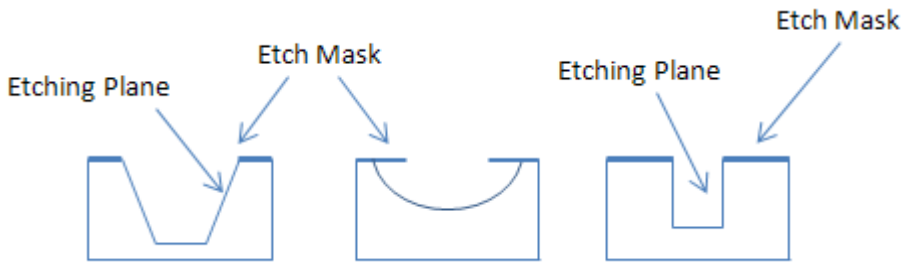

Fig. 5 Isotropic wet etch (left), anisotropic wet etch (middle) and DRIE straight wall etch (right)

With DRIE, the etching process is controlled and provides the fabrication of 90° angles. The process takes place at -15˚C and 33.75 mtorr and consists of alternating cycles of 6 seconds long of silicon etch and deposition of a chemically inert passivation layer; hexafluoride SF_6 as the

etchant and C_4F_8 as the protective layer. This alternation in cycles creates a scalloping pattern along the etched surface which is very small and negligible. This is called the Bosch process and is commonly used in the nanofabrication field. The wafers are etched at a rate of 10 µm/min. The downside of prolonged etch time is back deposit. It consists of a white residue on the wafer and is due to a combination of SF_6 and C_4F_8 and Si. This residue is not soluble in Acetone; we therefore use Oxygen Plasma Etch in order to remove the residue from the surface of the wafer.

The Oxygen Plasma Etch is an isotropic process which produces neutrally charged free oxygen radicals that react with the residue at the surface of the wafer. The oxygen has also a double action as it oxidizes the leftover photoresist and facilitates its removal; this process is referred to as *ashing*. The wafer is placed at a pressure of 100mtorr and a temperature of 25˚C for 15 minutes under plasma formed by 13.56 Mhz frequency for complete elimination of any molecules besides Si. Once this process is completed, the posts depth is measured by a profilometer with a very thin stylus (= µm) that allows a precise and accurate measurement of the depth since the spacing between the posts is much larger than the diameter of the stylus. Profilometers are commonly used in microfabrication in order to measure step heights and surface roughness. The machine consists of two major parts: a stage and a stylus. The wafer is placed on the stage and the stylus is dragged along the surface of the wafer. The vertical deflection measures the change in step height.[10]

2.3 Cleaning

The next step in the fabrication process consists of growing a thermal oxide layer on top of the wafer surface which will represent the semi-conducting layer. The wafer undergoes two cleaning processes known as Piranha Etch and RCA clean, prior to the oxide growth.

Piranha solution consists of a 2:1 mixture of 98% Sulfuric Acid H_2SO_4 and 30% Hydrogen Peroxide H_2O_2. The reaction between the two components is exothermic and the hydrogen peroxide is self-decomposing; the solution has to be freshly-mixed before use. Piranha etches away any organic component that might have resisted the plasma etch; the name of the solution comes from the ability to *eat away* everything. The sulfuric acid allows the removal of hydrogen and oxygen present in the molecule of water; this is called dehydration. The sulfuric acid present in the solution helps dissolve elemental carbon; this is done by dehydrating hydrogen peroxide molecules to form hydromium ions, bisulfate ions and atomic oxygen:

$$H_2SO_4 + H_2O_2 \rightarrow H_3O^+ + HSO_4^- + O$$

The atomic oxygen attaches directly to the targeted surface carbon in order to form a carbonyl group:

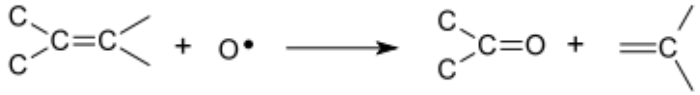

As shown above, the oxygen atom bonds with the central carbon, forming a carbonyl group and *setting-free* the targeted carbon. With further oxidation, the carbonyl group is transformed into a carbon dioxide:

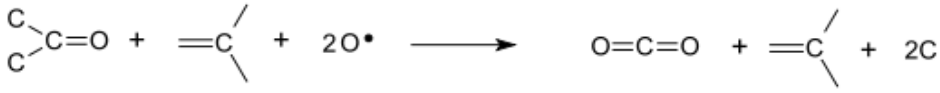

The targeted carbon can be a residue of the photolithography process or leftover from the piranha dehydration process. After the set time has elapsed, the piranha etch solution turns clear as all the residue evaporates in the form of carbon dioxide. This process results in a hydrophilic wafer

surface. We now take the substrate to the RCA cleaning bench.

Developed by an associate of the Radio Corporation of America (RCA), this cleaning procedure takes its name from the company. It is usually performed before high temperature processes such as oxidation, diffusion and chemical vapor deposition. RCA clean consists of three steps; removal of organic contaminant, removal of native oxides and removal of ionic contaminants. The wafers are first dipped in a diluted solution of 50:1 water H2O to Hydrogen Fluoride HF for 20 seconds then rinsed with De-Ionized (DI) water for one minute. They are then dipped in a solution known as SC-1 (Standard Cleaning), which consists of 15:2:1 Water H_2O, Hydrogen Peroxide H_2O_2 and Ammonium Hydroxide NH_4OH, for 10 minutes, heated at 60˚C. Once again the wafers go through the cycle of HF and DI water and finally dipped in SC-2 solution consisting of a 10:2:1 solution of H_2O, H_2O_2 and Hydrogen Chloride HCl for 10 minutes, heated at 60˚C before undergoing the cycle of HF and DI water one last time. The wafers are then dried with a flow of nitrogen and kept in a nitrogen box, to avoid recontamination, until the oxidation growth.

At this point the wafers are free of any organic and ionic contaminants, back deposit and photoresist. Indeed, the plasma etch, the Piranha etch and the RCA clean combined assure a wafer free of impurities that could impede the thermal oxide growth. The next step consists of growing the layer of oxide which will represent the semi-conducting layer of the posts.

The thermal oxidation is done at a specialized facility in the University of South Florida. In order to ease the oxidation process, the entire surface of the wafer is oxidized. Later on, a small part of the wafer is dipped in Buffered Oxide Etch BOE for 5 minutes in order to etch away the oxide and expose the bare silicon; this area will later be used for electrical contact. BOE is commonly used in microfabrication to etch away silicon dioxide. It is a very selective etch where it

stops at the silicon and does not etch it away[8].

2.4 Fluoropolymer Deposition

The wafers are finally inspected under the microscope to ensure the desired features; due to the size of the posts, we used Scanning Electron Microscope (SEM). SEM uses a high-energy beam of electrons (ranging from 0.5keV to 40 keV) in order to scan. The beam is focused through a series of condenser lenses to obtain a 0.4nm to 5nm diameter. The electrons interact with the surface of the wafer producing signals that contain information about the surface topography. SEM reveals high resolution images of features as small as 1 to 5 nm. It also allows a large range of magnification from 10 times the actual size to 500,000 times. The samples require a special prep before placing them in the microscope chamber.

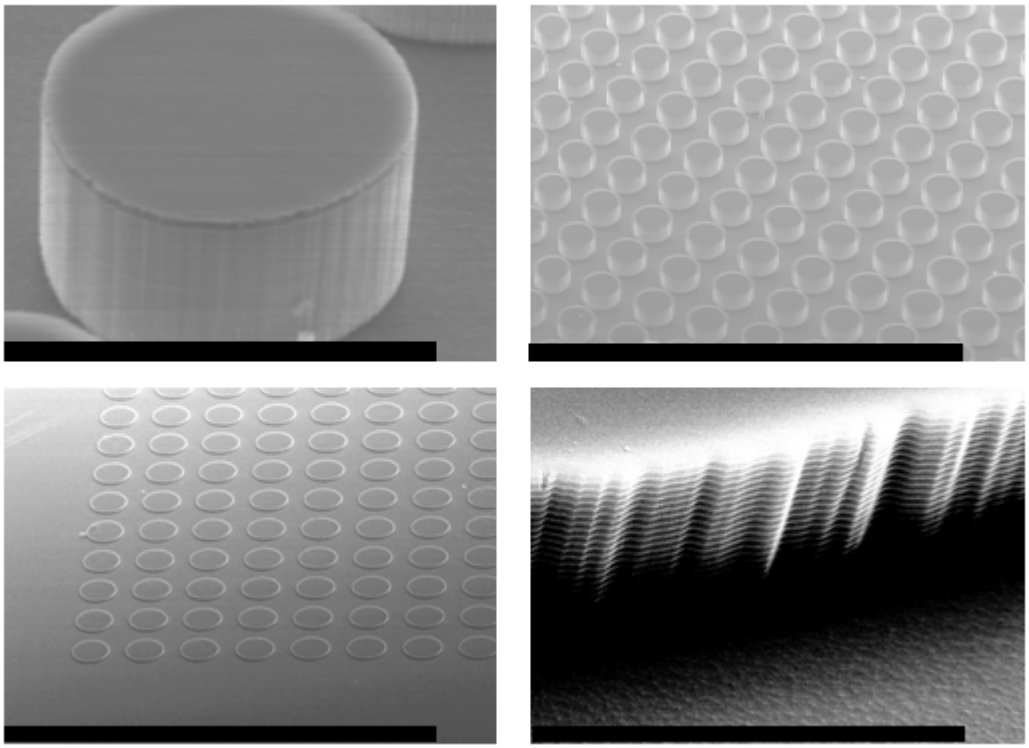

Fig. 6 SEM pictures

The wafers are nonconductive and tend to charge when in contact with the electron

beam causing false surface details. The wafers are therefore sputtered with gold which is considered a electrical conductor.

Indeed, we can see the scalloping on the walls of the posts caused by the DRIE process on fig. 6. The wafers are now transferred from the clean room to a regular laboratory in order to be processed. At this point of the process, the posts were etched to the desired depth and oxidized to form a thin semi-conductor layer. We now need to coat them with a fluoropolymer and prepare the setup for tests. The wafers are dip-coated in a diluted solution of 10:1 Isopropanol and commercial fluoropolymer for a period of five minutes. They are then baked in the oven for four minutes at 160˚C which allows the solvent to dry and the fluoropolymer to form a monolayer. The wafers are then transferred to the testing area.

3. Procedure & Results

3.1 Procedure

The goniometer for contact angle measurements consists of three main parts: a stage, a light source and an eye with microscope that can be interchanged with a camera in order to take pictures. A micrometer syringe filled with water is held on top of the stage and is used to drop 5µL droplets. First, the wafer is set on top of the stage which is adjusted to ensure a leveled surface. Then the eye lens which can be moved forward and backward in order to focus on the droplet is adjusted.

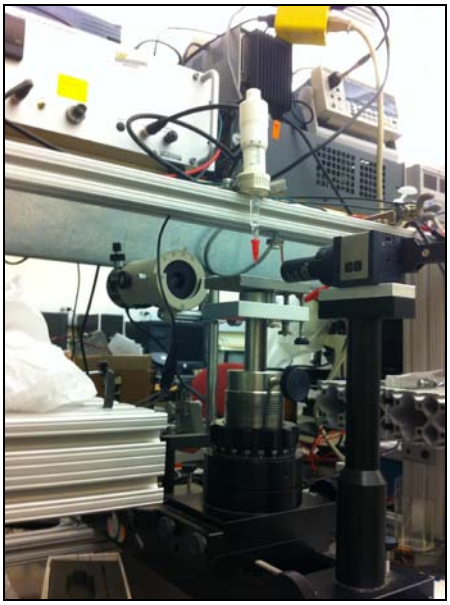

Fig. 7 Goniometer

Finally, the light which has several degrees of freedom is relatively adjusted to the camera to obtain high quality pictures. Once the droplet is dropped on top of the surface of the wafer, the experiment begins. The voltage source is setup next to the goniometer; the wafer is attached to the ground pole and the droplet to the positive pole of the voltage source. With 10mA intensity, the voltage is slowly increased to capture different wetting stages.

3.2 Results & Discussion

When setting up the experiment initially, a few tests of intensity change were performed, only to find out that intensity does not affect the wetting phenomenon in our case. The voltage is increased gradually; the step response occurs constantly at 100V, 200V and 300V on the 100 µm deep posts. On the 10 µm deep posts however, the response happens at lower voltages and that is due to the height of the posts. Two sets of data are considered to compare the theoretical to experimental results.

We consider a wafer of 10µm deep posts and a wafer with 100 µm deep posts. As shown in fig. 3 each wafer consists of arrays of different pitch and diameter dimensions. The roughness and Cassie coefficient of each set of dimensions is represented in the graph below:

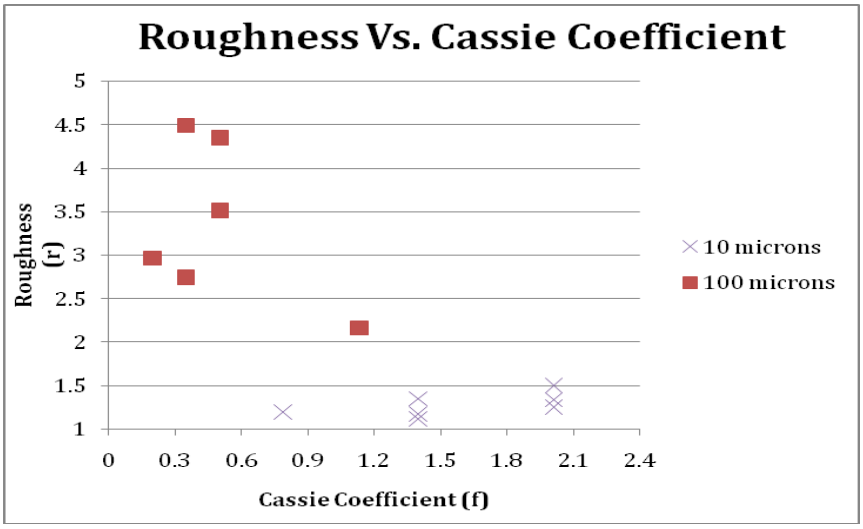

Fig. 8 Graph showing roughness versus Cassie coefficient

On the wafer, certain ratios of diameter to pitch were repeated for precision purposes. The calculations are shown in appendix 1. According to the theoretical results, the contact angle on 40X50, 80x100 and 60x75 arrays should be similar, same goes for 40x60 and 80x120 arrays.

The figures 9 and 10 below show picture results of water droplets sitting on arrays of different height and size.

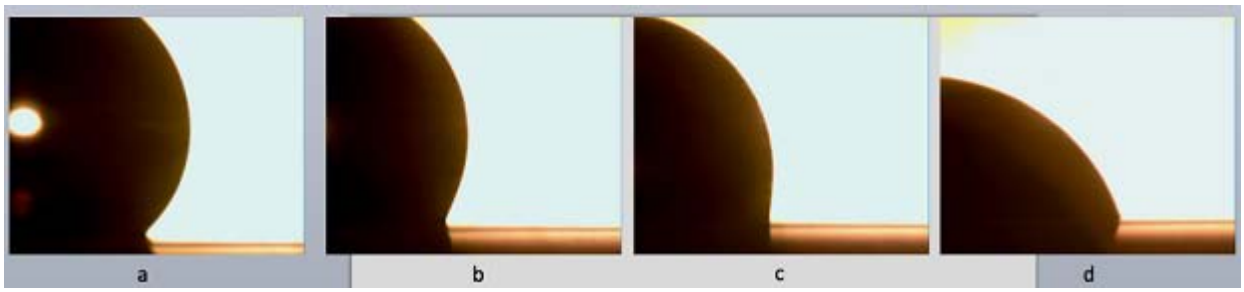

Fig. 9 Pictures of Cassie-Wenzel transition on 10µm deep posts. Contact angle measurement: a) 138 degrees, b) 112 degrees, c) 95 degrees, d) 63 degrees.

Picture (a) represents a droplet sitting on top of the posts in a Cassie state; the contact angle is measured at 138 degrees. The droplet does not wet the surface until a difference in potential of 100V is applied between the droplet and the wafer; the goniometer measures 112 degrees (picture b). The transition happens in milliseconds; it has been recorded in papers that it takes 17ms for the droplet to wet the surface. After 200V, the droplet wets the surface even more and the angle becomes 95 degrees (picture c). Finally at 300V, the droplet is in the Wenzel state forming 63 degrees between itself and the surface of the wafer (picture d). This first experiment proves the concept of electrowetting and shows the Cassie and Wenzel state.

We then test the 100µm deep posts and take pictures of the droplet transition in fig. 10.

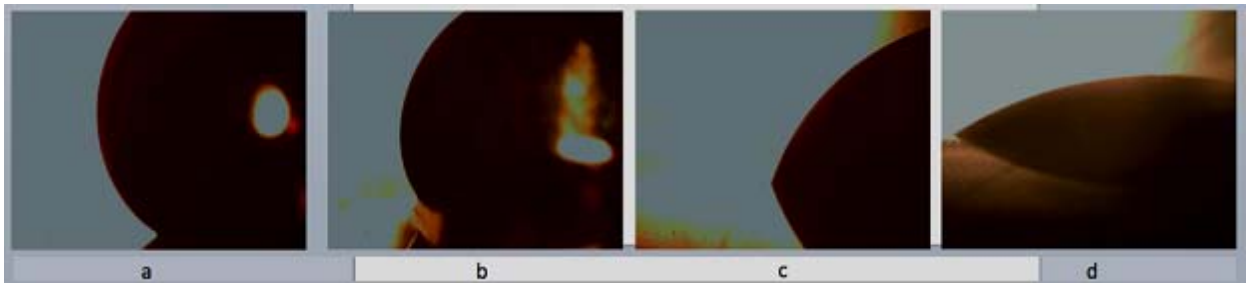

Fig. 10 Pictures of Cassie-Wenzel transition on 100µm deep posts. Contact angle measurement: a) 148 degrees, b) 122 degrees, c) 64 degrees, d) 33 degrees.

Picture (a) shows the droplet in Cassie state; the contact angle is measured at 148 degrees. When the difference in potential reaches 100V the contact angle becomes 122 degrees (picture b). After 200V, the droplet wets the surface further more and the angle becomes 64 degrees (picture c). Finally at 300V, the droplet is in a Wenzel state forming 33 degrees between itself and the surface of the wafer (picture d).

The set of data of contact angles recorded on different arrays on the 100µm posts are recorded in the table below:

Angle (deg) / Voltage (V)	40x50	40x60	40x80	60x75	80x100	80x120	120x180
0V	141	153	150	147	148	141	145
100V	130	133	125	134	134	123	122
200V	125	114	125	126	98	93	64
300V	48	33	30	53	51	34	35

Table. 1 Voltage versus angle response on 100 µm deep posts

The highest Cassie contact angle measured is 150 degrees on a 40x80 array and the lowest Wenzel angle measured is 30 degrees on the same array.

Comparing the 40x50 array results to the 60x75 and 80x100 (D:y=4/5) we see very similar transitions. While 120x180, 80x120 and 40x60 (D:y=2/3) varied highly when the difference of potential reached 200V and 300V. The images in fig. 9 and fig. 10 show different than the expected results and that is due to the fact that the pictures were taken on different arrays, where the 10 µm had a wider pitch; we therefore observed a higher Cassie angle in the 100 µm pictures.

The following graph and table show the results of the electrowetting transition on a 40x50 array, on both 10 µm and 100 µm posts.

Voltage (V)	0	50	100	170	190	200	300
Angle on 10 µm	138	98	-	64	50	30	-
Angle on100 µm	141	-	130	-	-	125	48

Table 2. Angle measurements on both 10 µm and 100 µm deep posts

We then plot the expected contact angle versus the experimental reading on 10 µm and 100 µm deep posts. Fig. 11 shows the plots of 10 µm deep posts.

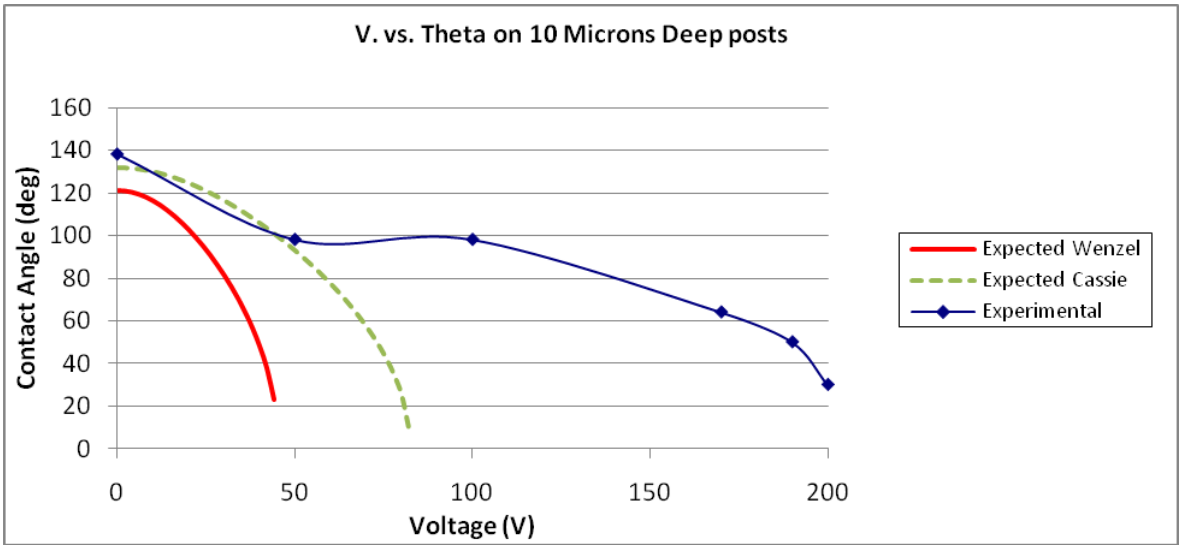

Fig. 11 Expected Cassie, expected Wenzel and experimental results of voltage versus contact angle on 10 µm deep posts

As we can see, the expected values respond to a smaller difference in potential than the actual results; the plot trend however is similar. The experimental results curve expands on a larger range of voltage values. The contact angle at 0V and the saturation angle are very close.

Fig. 12 shows the plots on 100 µm deep posts. The experimental results are very similar to the expected Cassie curve. As for the 10 µm deep posts, the contact angles are similar to the extent that they respond to a wider range of contact angles.

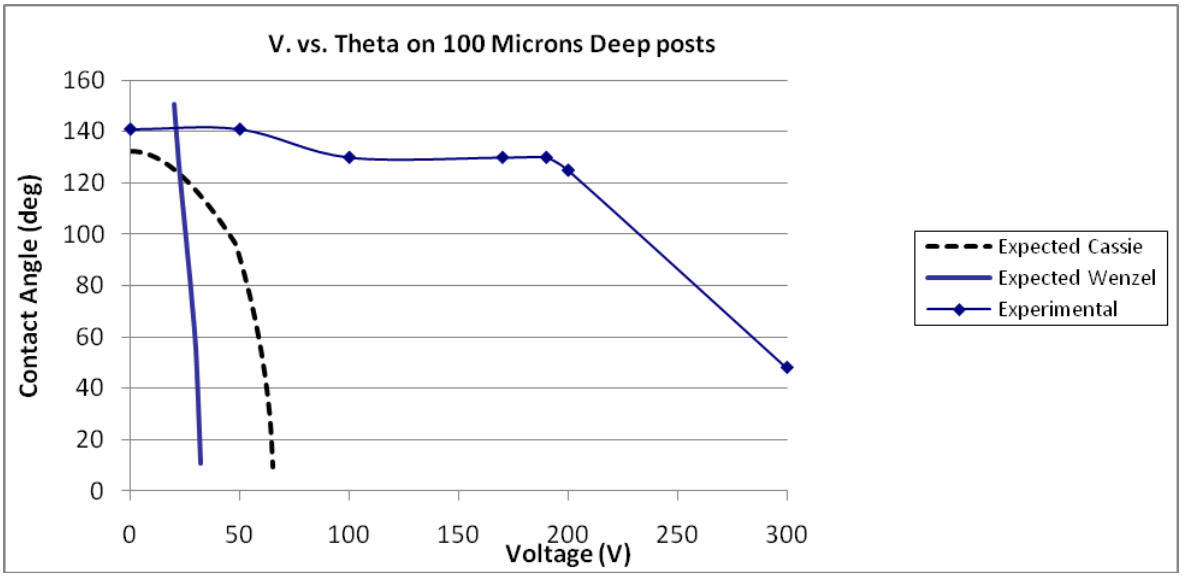

Fig. 12 Expected Cassie, expected Wenzel and experimental results of voltage versus contact angle on 100 µm deep posts

4. Conclusion

The electrowetting structure consisting of a water droplet sitting on commercial fluoropolymer dielectric coated substrate charged by a Direct Current (DC) voltage source, demonstrated the Cassie and Wenzel laws. Energy minimization, interfacial thermodynamics and electromechanics were used to predict theoretical results.

We can see from the results in table 2. a match with the eq. 10 where the greater transition angle happens on the smaller height posts. On smaller posts however, once the first wetting stage is attained, there is a need of smaller difference in potential in order to achieve the Wenzel state.

Arrays with similar diameter to pitch ratio tend to react in a similar way to a specific difference in potential, as it was shown in table 1., which is due to the fact that both diameter (d) and pitch (y) are present in the equation for roughness and Cassie coefficient equations (eq. 11, 12) which in turn are present in the Cassie and Wenzel angle equations (eq. 8, 9).

Fig. 11 and 12 show that the experimental results are similar to the expected results, to the extent that the drop responds to a higher difference in potential in the experiment. This difference in voltage can be due to imperfections in the thermal oxide growth process.

Experimental results have indeed matched the theoretical expectations. We can therefore proceed with implementing these wafers in different applications. One of the potential and highly needed research projects is the reversibility of the Electrowetting effects; in other words applying voltage or current in order to take the droplet back from the Wenzel state to the Cassie state. Research has been done in this field however, a perfect trigger has not been found yet. Some use an electrical trigger that leads to the heating of the substrate turning the water into gas, creating a

small area where the contact forces are very low[5]. This pushes the droplet back to the top of the surface. This technique boils some of the water and therefore the droplet is not recovered completely. Others have found that a drop of oil allows the transition, yet this technique contaminates the substrates and makes it non-reusable[1]. We therefore need a trigger that preserves the initial volume of the droplet and does not contaminate the substrate.

References

[1] Heikenfeld, J.;Dhindsa, M, Electrowetting on Superhydrophobic Surfaces: Present Status and Prospects. Journal of Adhesion Science and Technology 2008, 22, 319-334.

[2] Krupenkin, T. N.; Taylor, J. A.; Schneider, T. M.; Yang, S., From Rolling Ball to Complete Wetting: The Dynamic Tuning of Liquids on Nanostructured Surfaces. Langmuir 2004, 20 (10), 3824-3827.

[3] Swain, P. S.; Lipowsky, R., Contact Angles on Heterogeneous Surfaces: A New Look at Cassie's and Wenzel's Laws. Langmuir 1998, 14 (23), 6772-6780.

[4] Lapierre, F.; Thomy, V.; Coffinier, Y.; Blossey, R.; Boukherroub, R., Reversible Electrowetting on Superhydrophobic Double-Nanotextured Surfaces. Langmuir 2009, 25 (11), 6551-6558.

[5] Krupenkin, T. N.; Taylor, J. A.; Wang, E. N.; Kolodner, P.; Hodes, M.; Salamon, T. R., Reversible Wetting−Dewetting Transitions on Electrically Tunable Superhydrophobic Nanostructured Surfaces. Langmuir 2007, 23 (18), 9128-9133.

[6] Berthier, Jean. Micro-drops and Digital Microfluidics. Chap. 3 Sec. 3.3.3. Burlington: Elsevier, 2008. Internet resource.

[7] Patankar, N. A., Hysteresis with Regard to Cassie and Wenzel States on Superhydrophobic Surfaces. Langmuir 2010, 26 (10), 7498-7503.

[8] “Wet Oxide Etch.” Colorado School of Mines Website, 22 Mar. 2011. <http://inside.mines.edu/~sagarwal/phgn435/BOE.html>

[9] “Photolithography.” School of Electrical and Computer Engineering, 22 Mar. 2011. <http://www.ece.gatech.edu/research/labs/vc/theory/photolith.html>

[10] “Profilometer.” Stanford Nanofabrication Facility, 22 Mar. 2011. <http://snf.stanford.edu/>

[11] Findenegg, G. H.; Herminghaus, S. *Curr. Opin. Colloid Interface Sci.* **1997**, *2*, 301. Blokhuis, E. M.;Widom,B. *Curr. Opin. Colloid Interface Sci.* **1996**, *1*, 424. Forgacs, G.; Lipowsky, R.; Nieuwenhuizen, T. M. In *Phase Transitions and Critical Phenomena*; Domb, C., Lebowitz, J. L., Ed.; Academic Press: London, 1991.

[12] Wenzel, R. N. *J. Phys. Colloid Chem.* **1949**, *53*, 1466; *Ind. Eng. Chem.* **1936**, *28*, 988.

[13] Cassie, A. B. D. *Discuss. Faraday Soc.* **1948**, *3*, 11.

[14] Borgs, C.; de Coninck, J.; Kotecky´ , R.; Zinque, M. *Phys. Rev. Lett.***1995**, *74*, 2292.

[15] Parry, A. O.; Swain, P. S.; Fox, J. A. *J. Phys. Condens.: Matter***1996**, *8*, L659. Swain, P. S.; Parry, A. O. *J. Phys. A* **1997**, *30*, 4597. Swain, P. S.; Parry, A. O. *Eur. Phys. J. B* **1998**, *4*, 459.

[16] Urban, D.; Topolski, K.; de Coninck, J. *Phys. Rev. Lett.* **1996**, *76*, 4388.

[17] Toshev, B. V.; Platikanov, D.; Scheludko, A. *Langmuir* **1988**, *4*, 489.

[18] Drelich, J.; Miller, J. D. *Langmuir* **1993**, *9*, 619.

[19] Drelich, J. *Colloids Surf. A* **1996**, *116*, 43.

[20] Young, T. *Philos. Trans. R. Soc. London* **1805**, *95*, 65.

[21] Shibuichi, S.; Onda, T.; Satoh, N.; Tsujii, K. *J. Phys. Chem.* **1996**, *100*, 19512.

[22] Miwa, M.; Nacajima, A.; Fujishima, A.; Hashimoto, K.; Watanabe, T. *Langmuir* **2000**, *16*, 5754.

[23] Chen, W.; Fadeev, A.; Hsieh, M. C.; Oner, D.; Youngblood, J.; McCarthy, T. J. *Langmuir* **1999**, *15*, 3395.

[24] Youngblood, J. P.; McCarthy, T. J. *Macromolecules* **1999**, *32*, 6800.

[25] Inoue, Y.; Yoshimura, Y.; Ikeda, Y.; Kohno, A. *Colloids Surf., B* **2000**, *19*, 257.

[26] Matsumoto, Y.; Ishida, M. *Sens. Actuators* **2000**, *83*, 179.

[27] Hozumi, A.; Takai, O. *Thin Solid Films* **1997**, *303*, 222.

[28] Bico, J.; Marzolin, C.; Quere, D. *Europhys. Lett.* **1999**, *47*, 220.

[29] Nakejima, A.; Hashimoto, K.; Watanabe, T. *Monatsh. Chem.* **2001**, *132*, 31.

[30] Lafuma, A.; Quere, D. *Nat. Mater.* **2003**, *2*, 457.

[31] Ichimura, K.; Oh, S.-K.; Nakagawa, M. *Science* **2000**, *288*, 1624.

[32] Lahann, J.; Mitragotri, S.; Tran, T.-N.; Kaido, H.; Sundaram, J.; Choi, I. S.; Hoffer, S.; Somorjai, G.; Langer, R. *Science* **2003**, *299*, 371.

[33] Isaakson, J.; Tengstedt, C.; Fahlman, M.; Robinson, N.; Berggren, M. *Ad*V. *Mater.* **2004**, *16*, 316.

[34] Krupenkin, T.; Taylor, J.; Schneider, T.; Yang, S. *Langmuir* **2004**, *20*, 3824.

[35] Sun, T.; Wang, G.; Feng, L.; Liu, B.; Ma, Y.; Jiang, L.; Zhu, D. *Angew. Chem.* **2004**, *43*, 357.

[36] Krupenkin, T.; Taylor, J. A.; Kolodner, P.; Hodes, M. *Bell Labs Techn. J.* **2005**, *10*, 161.

[37] Cassie, A. B. D.; Baxter, S. *Trans. Faraday Soc.* **1944**, *40*, 546.

[38] Wenzel, R. N. *J. Phys. Colloid Chem.* **1949**, *53*, 1446.

[39] He, B. H.; Patankar, N. A.; Lee, J. *Langmuir* **2003**, *19*, 4999.

[40] 124 Vaibhav Bahadur and Suresh V. Garimella, "Electrowetting-based control of static droplet states on rough surfaces," Langmuir 23 (9), 4918 (2007).

[41] 125 Wei Dai and Ya-Pu Zhao, "An electrowetting model for rough surfaces under low voltage," J.Adhes.Sci.Technol. 22 (2), 217-29 (2008).

Appendix A

$$r = 1 + \frac{\pi\left(\frac{d}{H}\right)}{y^2} \qquad \text{Eq. (14)}$$

$$f = \frac{\pi\left(d^2\right)}{4y^2} \qquad \text{Eq. (15)}$$

Height (H)	100	100	100	100	100	100	100
Diameter (d)	40	40	40	80	80	120	60
Pitch (y)	50	60	80	100	120	180	75
Roughness (r)	6.028571	4.492063	2.964286	3.514286	2.746032	2.164021	4.352381
Cassie Coefficient (f)	0.502857	0.349206	0.196429	0.502857	0.349206	0.349206	0.502857

Table A.1 Roughness and Cassie Coefficient for 10 µm deep posts

Diameter (d)	40	40	40	80	80	120	60
Pitch (y)	50	60	80	100	120	180	75
Roughness (r)	6.028571	4.492063	2.964286	3.514286	2.746032	2.164021	4.352381
Cassie Coefficient (f)	0.502857	0.349206	0.196429	0.502857	0.349206	0.349206	0.502857

Table A.2 Roughness and Cassie Coefficient for 100 µm deep posts

Diameter (d)	40	40	40	80	80	120	60
Pitch (y)	50	60	80	100	120	180	75
Diameter : Pitch (D:y)	4/5	2/3	1/2	4/5	2/3	2/3	4/5

Table A.3 Ratios of diameter to pitch

Appendix B

Tables B.1 and B.2 show samples of the expected Cassie and Wenzel contact angles:

Voltage (V) / Angle (deg)	0	10	20	30	40	50	60
Cassie	132.14	130.26	124.91	116.68	106.05	93.13	77.49
Wenzel	120.93	116.09	102.56	81.20	47.80	-	-

Table B.1 Expected Cassie and Wenzel angles versus Voltage on 10 µm

Voltage (V) / Angle (deg)	0	10	20	30	40	50	60
Cassie	132.14	130.26	124.91	116.68	106.05	93.13	77.49
Wenzel	-	-	150.79	52.16	-	-	-

Table B.2 Expected Cassie and Wenzel angles versus Voltage on 100 µm